Modeling of corundum breakdown textures in anorthosite from the Sittampundi layered magmatic complex, South India

By
Arnab Dey
Examination roll no. MGEO194014
Dept. of Geological Sciences
Jadavpur University

Modeling of corundum breakdown textures in anorthosite from the Sittampundi layered magmatic complex, South India

Thesis submitted for partial fulfillment of M.Sc. Degree in Applied Geology 2019

by

Arnab Dey

Registration no-128281 of 2014-15

Class roll no- 001720402013

Examination roll no-MGEO194014

Department of Geological Sciences

Jadavpur University

Under guidance of Prof. Pulak Sengupta

Department of Geological Sciences

Jadavpur University

যাদবপুর বিশ্ববিদ্যালয়
কলকাতা-৭০০০৩২, ভারত

JADAVPUR UNIVERSITY
KOLKATA-700032, INDIA

FACULTY OF SCIENCE : DEPARTMENT OF GEOLOGICAL SCIENCES

CERTIFICATE FROM THE SUPERVISOR

This is to certify that **Mr. Arnab Dey** has worked under the supervision of Prof. Pulak Sengupta in the Department of Geological Sciences, Jadavpur University and completed his thesis entitled **"Modeling of corundum breakdown textures in anorthosite from the Sittampundi layered magmatic complex, South India"** which is being submitted towards the partial fulfillment of his M.Sc. Final Examination in Applied Geology of Jadavpur University in 2019.

Signature of the Supervisor:

Prof. Pulak Sengupta
Dept. of Geological Sciences
Jadavpur University

Dr. Pulak Sengupta
Professor
Department of Geological Sciences
Jadavpur University, Kolkata-700032

Signature of Head of the Department:

30/05/2019

Prof. Sanjoy Sanyal
Dept. of Geological Sciences
Jadavpur University

Head
Department of Geological Sciences
Jadavpur University
Kolkata-700032

দূরভাষ : ২৪১৪-৬৬৬৬/প্রসারণ : ২২৬৮
Website : www.jadavpur.edu
E-mail : hod_geological@jdvu.ac.in
Phone : 2414 6666/Extn. 2268

Scanned with CamScanner

Dedicated to my parents, who were always by my side

Contents

MODELLING OF CORUNDUM BREAKDOWN TEXTURES IN ANORTHOSITE FROM THE SITTAMPUNDI LAYERED MAGMATIC COMPLEX, SOUTH INDIA.

Abstract

The highly calcic anorthosite (An>95) from the Sittampundi Layered Complex (SLC) develops corundum, spinel and sapphirine. The SLC is a magmatic-layered complex consisting of an interlayered sequence of anorthosite, chromite-bearing clinopyroxenite, and chromite-free mafic-ultramafic rocks. The members of the SLC were emplaced at ~2.8–2.9 Ga and were subsequently metamorphosed at ~ 2.48 Ga under granulite-facies conditions (~12 kbar, ~800 °C) with a steep decompressive retrograde P-T-path (~7 kbar, ~730 °C).

The studied anorthosite is milky white and highly recrystallized imparting a saccharoidal appearance. It contains laterally discontinuous dark bands of amphibole. Locally, millimeter- to centimeter-thick discontinuous layers of corundum are found in the anorthosite.Corundum is always separated from amphibole by successive coronae of green spinel (proximal to corundum) and plagioclase (toward the amphibole-plagioclase matrix). Sapphirine forms around spinel making the contact between anorthite and corundum highly irregular. The textures indicate the following sequence of mineral growth:

$plagioclase_{matrix}$ → corundum; corundum + amphibole → $plagioclase_{corona}$+ spinel; and spinel + corundum → coronitic sapphirine.

Topological constraints in parts of the Na_2O–CaO–MgO–Al_2O_3–SiO_2–H_2O (NCMASH) system suggest that aqueous fluid(s) permeated the rock and the assemblage corundum + amphibole + anorthite ± clinozoisite was stabilized during high-pressure (HP) metamorphism (11 ± 2 kbar, 750 ± 50 °C). Constraints of the NCMASH topology also suggest that coronitic plagioclase and spinel formed at the expense of corundum + amphibole during a steeply decompressive retrograde *P–T* path (7–8 kbar and 750 ± 50 °C) in an open system. Chemographic projections in the MAS system, combined with textural modeling studies support the view that the peraluminous sapphirine formed from due to silica and Mg metasomatism of the precursor spinel + corundum, on the steeply decompressive retrograde *P–T* path. Extremely channelized fluid flow and the positive solid volume change of the stoichiometrically balanced sapphirine forming reaction explains the localized growth of sapphirine.

1. Introduction:

Corundum from anorthositic mafic rocks has been reported from few areas of diverse geological settings (Schreyer et al 1981; Ranson 2000; Morishita et al 2004).However, the origin of corundum in mafic/ultramafic rocks has been a subject of considerable debate. The opinion varies from magmatic crystallization at high-pressure (Sen and Presnall 1984; Liu and Presnall 1990)-to-UHP metamorphism at mantle depth (Morishita and Kodera 1998; Morishita 2004) to crustal anatexis of anorthosite (Kullerud et al. 2012).Metasomatic origin of sapphirine in different rock types at temperatures <800°C has been reported from a few localities (Peck and Valley 1996; Dunkley et al. 1999; Fernando 2001; Tenthorey et al. 1996; Sengupta et al. 2004; Raith et al. 2008). However, corundum–spinel–sapphirine-bearing aluminous assemblages from basic to ultrabasic complexes have been reported from only one locality, Variscan French Massif Central (Berger et al. 2010).The factors that controlled the stability of the atypical peraluminous minerals (corundum, spinel, sapphirine etc.) in rocks of basic–ultrabasic compositions are not well understood.

In the Indian shield, the assemblage corundum–sapphirine has been reported only from the Sittampundi Layered (Magmatic Complex (SLC), south India (Subramaniam 1956; Ashwal 1993). Within the scope of my dissertation work rare ensemble of peraluminous minerals (corundum, spinel and sapphirine) in the highly calcic anorthosite from the late Archean SLC has been studied. An attempt has been made to explain the breakdown of corundum to spinel and sapphirine.

Disequilibrium between host rock and percolating fluid commonly leads significant changes of host rock composition (Dutrow et al 1999,2008; Phillpots and Ague 2009; Chowdhury et al 2013).Using chemographic plots, textural modeling using the computer program CSpace (Torres-Roldan et al. 2000), and thermodynamic analyses in parts of the NCMASH (Na_2O-CaO-MgO–Al_2O_3–SiO_2–H_2O) system using the computer program Perplex (Connolly 2005; 2009), it has been demonstrated that spinel and sapphirine in the SLC were developed due to metasomatic alteration of a Neoarchean (~2.8– 2.9 Ga) oceanic crust during ~2.45 Ga high-pressure (HP) metamorphism. Such studies provide valuable information about the nature and mechanism of metasomatic modification of the host rock in terms of pressure, temperature and composition of the permeating supercritical fluids in the zones of high fluid flux such as oceanic crust, mantle wedge above the subduction zone, etc.(Phillpots and Ague 2009).

2. Geological background:

The granulite terrain of south India is considered to be a mosaic of crustal domains with distinctive geological and geochronological characteristics (Bhaskar Rao et al., 2003; Braun and Kriegsman, 2003; Ghosh et al., 2004). A number of crustal-scale shear zones are presumed to have divided the entire granulite belt into three major domains (Fig. 1). The northernmost domain, the northern granulite terrains (NGT), exposes an assemblage of mafic, ultramafic and volumetrically major felsic orthogneisses that underwent a last high-grade event at ca. 2.6–2.5 Ga, whereas the southern most domain (Madurai Block or MB) shows a last high-grade event at a much younger age (ca. 0.6–0.5 Ga; Bhaskar Rao et al., 2003; Braun and Kriegsman, 2003; Chetty,1996; Chetty et al., 2003; Ghosh et al., 2004). The NGT and MB are separated by a roughly E–W trending belt. The rock associations in this belt show complex magmatic, metamorphic and deformational history over a protracted period from 2.9 Ga to 0.5 Ga (Bhaskar Rao et al., 2003; Braun and Kriegsman, 2003; Ghosh et al., 2004; Mukhopadhyay et al., 2003; Raith et al., 2010). Several crustal-scale shear zones are believed to have affected the rocks of this linear belt for which is often referred to as the Cauvery Shear System (CSS, Chetty, 1996; Fig. 1).

The first systematic study on the rocks of SLC was done by Subramanium (1956). Existing geochronological data indicate that the layered complexes were emplaced at ca. 2.9 Ga (Bhaskar Rao et al., 1996; Ghosh et al., 2004; Subramanium, 1956). A suite of felsic magmas now represented by enderbite and charnockite (felsic orthogneiss) subsequently intruded the members of the SLC. The entire ensemble of mafic, ultramafic and felsic rocks underwent deformation accompanied by high-grade metamorphism at ca. 2.40– 2.45 Ga and by amphibolite facies metamorphism during ca. 0.72– 0.50 Ga (Bhaskar Rao et al., 1996; Ghosh et al., 2004; Meissner et al. 2002). Late Archaean and Neoproterozoic tectonothermal activities obliterated the primary magmatic features of the layered complexes in most places although vestiges of rhythmic inter layering among anorthosite, chromitite and clinopyroxenite are present and are considered to be of magmatic origin (Subramanium, 1956).

The generalized geological map of the SLC showing dispositions of the different lithologies is presented in Fig. 1. The rocks of this magmatic complex and the adjoining areas have been studied by a number of authors (Bhaskar Rao et al., 1996, 2003; Ghosh et al., 2004; John et al., 2005; Mukhopadhyay et al., 2003; Ramadurai et al., 1975; Sengupta et al.,

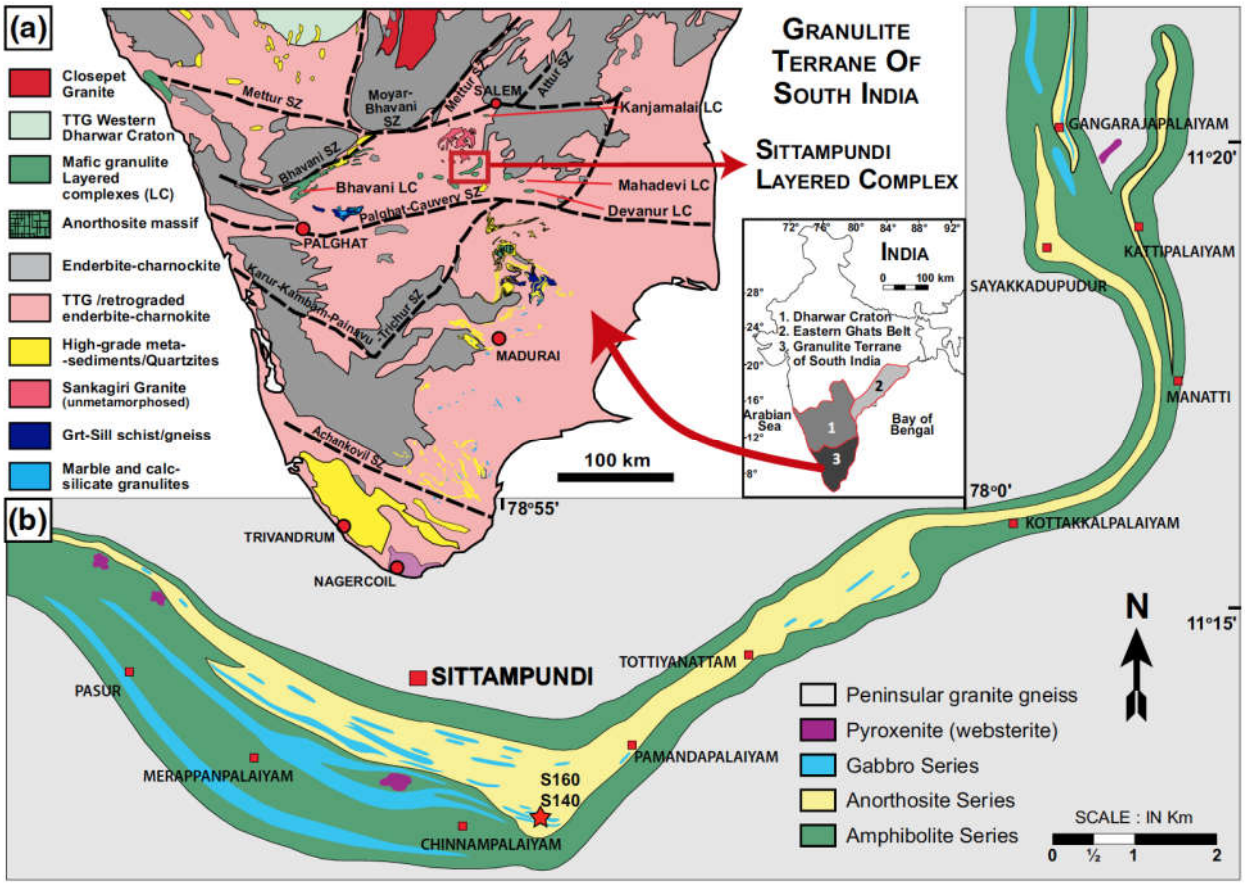

Fig 1.(a) Regional lithological map of the Southern Granulite Terrane (Karmakar et al 2017).(b) Different lihological units of Sittampundi Layered Complex.

2009a,b; Shimpo et al., 2006; Subramanium, 1956, among others). The SLC comprises an intercalated sequence of clinopyroxenite, anorthosite and a suite of mafic rocks now represented as mafic granulite with the mineralogy clinopyroxene+ plagioclase± orthopyroxene ±garnet ±amphibole (Bhaskar Rao et al., 1996; Ghosh et al., 2004; our unpublished data). Although dm to cm-thick chromitite layers are present in clinopyroxenite and anorthosite, thick bands (up to 6 meter thick, Subramanium, 1956) of economic-grade chromite occur only in clinopyroxenite (now extensively retrograded to amphibolite). Extant geochemical and Nd-isotope data indicate that the mafic– ultramafic rocks of the SLC are co-genetic and show a fractionation trend akin to that of tholeiitic magma (Bhaskar Rao et al., 1996). A ca. 2.9 Ga emplacement age for the SLC has been established by whole-rock Sm–Nd isochron and U–Pb dating of zircon (Bhaskar Rao et al., 1996; Ghosh et al., 2004). Vestiges of Banded Iron Formation (BIF), which represent the sole sedimentary component in the magmatic sequence and are intimately associated with the mafic rocks of the SLC. The SLC is surrounded by felsic orthogneiss (ca. 2.51 Ga emplacement age; Ghosh et al., 2004), which contains fragments of mafic ultramafic rocks including xenoliths of dunite, harzburzite and wherlite, and sends apophyses into the rocks of the magmatic complex. Features such as (a) occurrence of chromite-bearing ultramafic enclave in mafic rocks, and (b) presence of tongues of mafic rocks in anorthosite corroborate the view that mafic rocks represent the uppermost part of the SLC. Intimate association of mafic rocks with BIF which is presumed to have deposited as chemical sediments also corroborates this view.

3. Mesoscopic features:

The samples contain milk-white anorthosite layers that alternate with millimeter to decimeter thick layers rich in amphiboles (Fig2 A). A prominent planer fabric that is parallel to the penetrative foliation is defined by alignment of amphibole grains (Fig 2 A,E). However random orientation of a few amphibole suggest the foliation of amphibole outlasted the deformation (Fig 2 B). Recrystallization of anorthite imparts a saccharoidal appearance to the rock.

Colourless to pink colour corundum are also found in the rock samples (Fig. 2 C-E). The long axis of the corundum grains are oriented parallel to the foliation. In the vicinity of chromite bearing layers, corundum shows a pink colour (ruby). The grains are fractured and

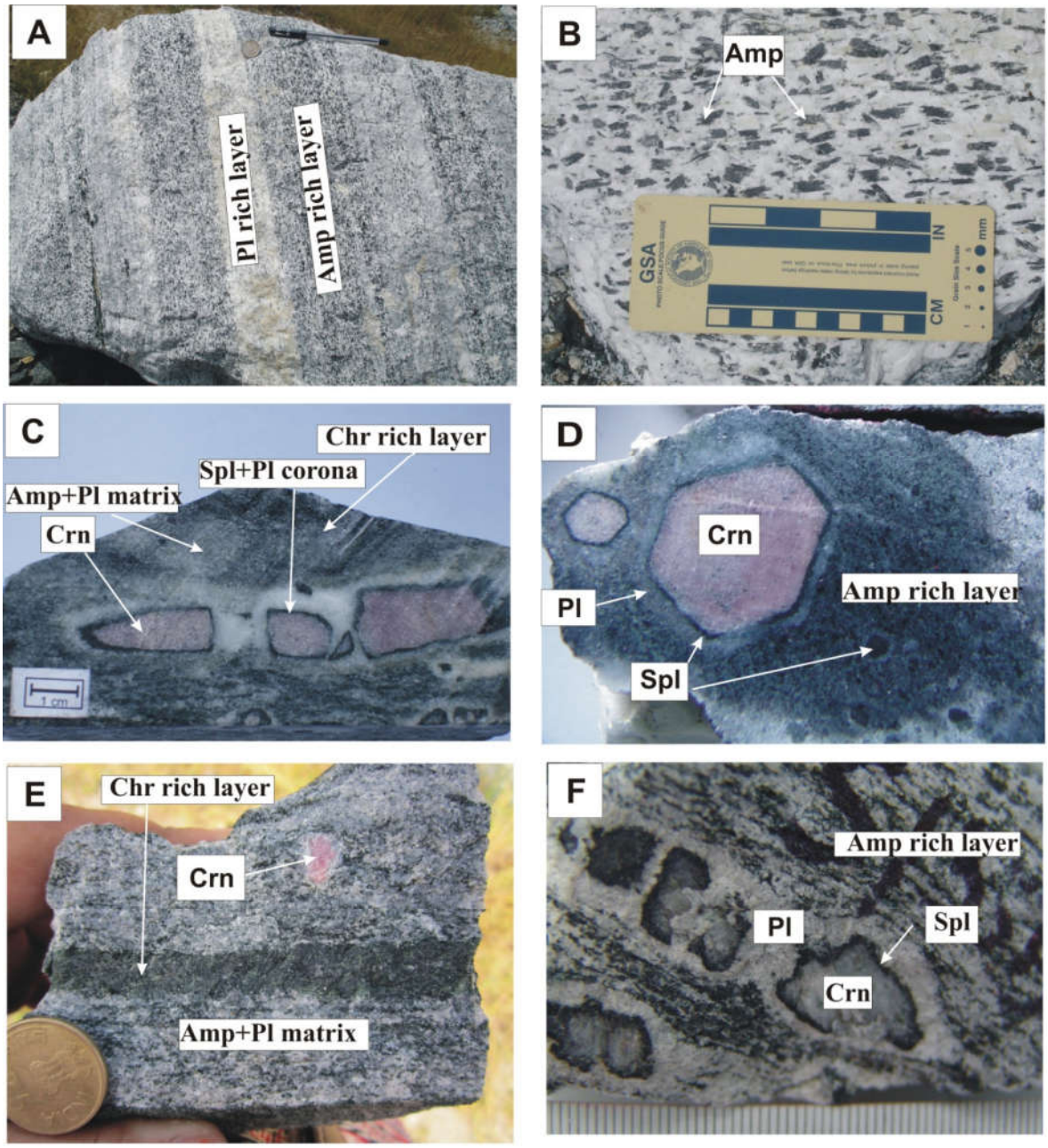

Fig 2. Field and hand specimen photographs. (A) Alternative Amp rich layer and Pl rich layer of anorthosite of SLC. (B) Haphazard orientation of Amp in anorthosite. (C) Crn is surrounded by corona of Spl+Pl within the Amp+Pl matrix. The Crn is elongated and showing boudinuge structure. (D) Hexagonal pink Crn is surrounded by Spl+Pl in Amp rich layer. In the layer there are some Spl which completely replaces Crn. (E) Pink Crn is placed in the matrix of Pl and Amp. The Crn is separated from the matrix by a thin corona of only Pl. (F)White colored Crn is separated from the matrix by corona of Spl and Pl.

showing boudinuge structure (Fig 2 C). Also hexagonal basal section (0001 plane) is found (Fig 2 D). The corundum grains are commonly surrounded by thin corona of spinel and separated from the amphibole rich layer by a corona of plagioclase (Fig 2C-F). Some of the corundum grains are fully replaced by spinel. The interface between the spinel and the corundum is sharp.

4. Petrography:

I studied total 10 samples under microscope. The rock contains amphibole (Amp), plagioclase (Pl), corundum (Crn), spinel (Spl), sapphirine (Spr) and opaque (Opq) minerals. The amphiboles are prismatic in shapes, which define crude foliation (Fig. 3 B,C). Amphibole and plagioclase together define a recrystallized granoblastic texture, where grain boundaries are at an angle of 120° triple junctions, (Fig. 3 B,C). Some of the amphibole is randomly oriented, which does not show any internal deformation, suggesting the mineral growth outlasts the deformation. Subhedral-anhedral corundum grains occurin the matrix of plagioclase + amphibole (Fig. 3 D,F-J). Corundum is separated from the matrix by either corona of spinel, sapphirine and plagioclase (Fig. 3 F-H) or corona of spinel and plagioclase (Fig. 3D) or symplectite intergrowh of plagioclase+spinel (Fig. 3 G,H). The width of double corona of spinel+plagioclase as well as sapphirine varies. The proportion of spinel is decreasing away from the corundum (Fig.3 G,H). In the symplectites, spinel grains are anhedral, elongated in shape oriented perpendicular to the grain boundary of corundum (Fig. 3G,H). In some cases corundum is fully replaced by spinel forming pseudomorphs (Fig. 3E). Development of thin corona indicates early stages of replacement but the complete pseudomrph indicates advanced stage of replacement. In some cases spinel is surrounded by a thin corona of sapphirine suggesting sapphirine is formed after the formation of spinel. The sapphirine formation is very restricted and it is not formed in all cases (Fig. 3 I,J).The corundum contains inclusions of plagioclase, suggesting corundum has formed after the formation of plagioclase (Fig. 3F). At the boundary of spinel there is also corundum and magnetite (Mag) indicating that spinel breaks down to corundum magnetite.

From the textural evidences the following sequences of mineral growths can be concluded:

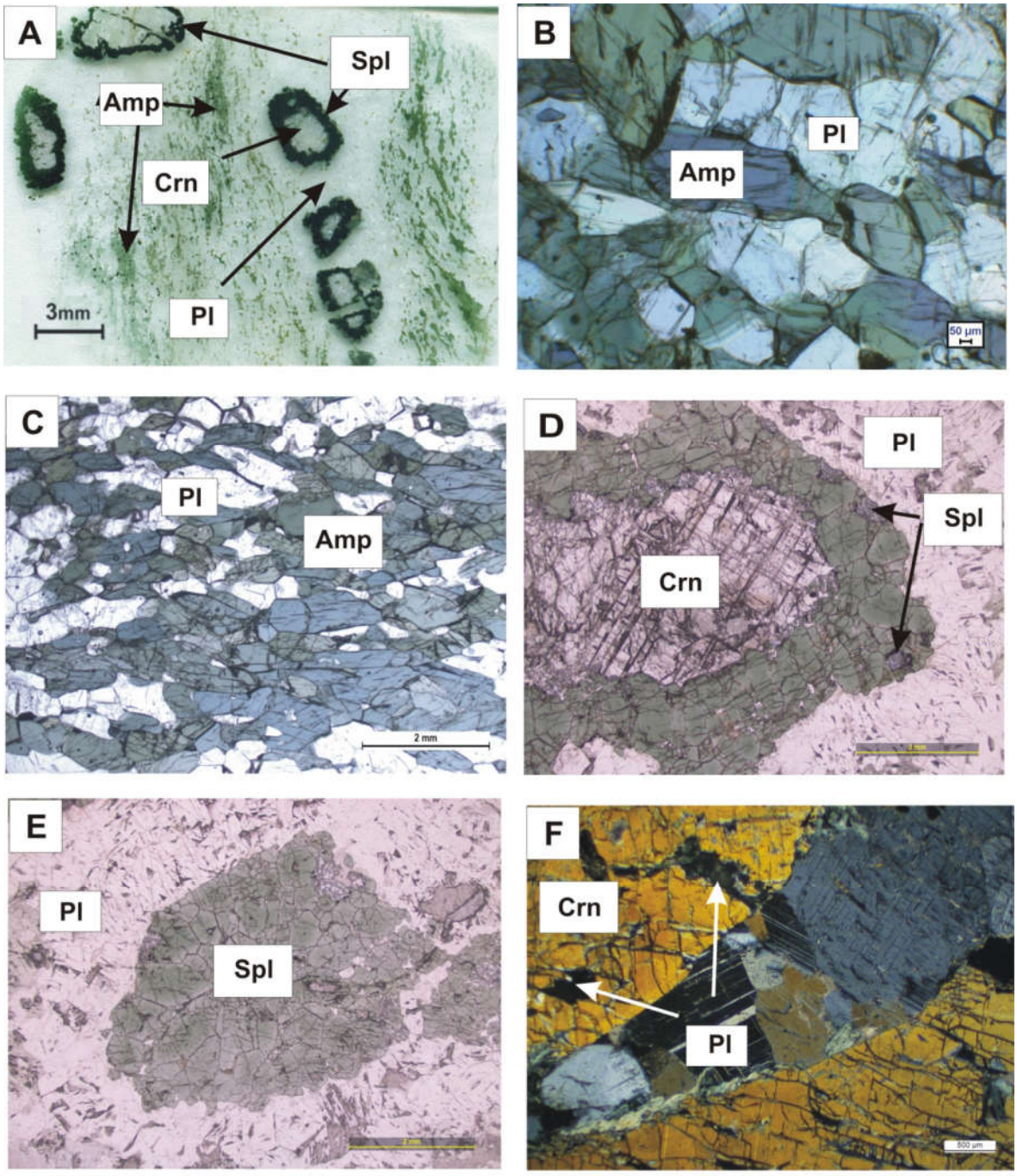

Fig3. Photomicrographs showing textural relations. (A)Scanned image of a thin section showing Crn is surrounded by double corona of Spl and Pl placed in the matrix of Amp+Pl. (B, C)Amp and Pl in the matrix showing recrystallized granoblastic texture and defining crude foliation in the rock(PPL) (D)Crn is surrounded by corona of Spl in the Pl matrix.(E) Spl completely replaces the Crn forming pseudomorph, (F) Inclusion of Pl in the Crn.

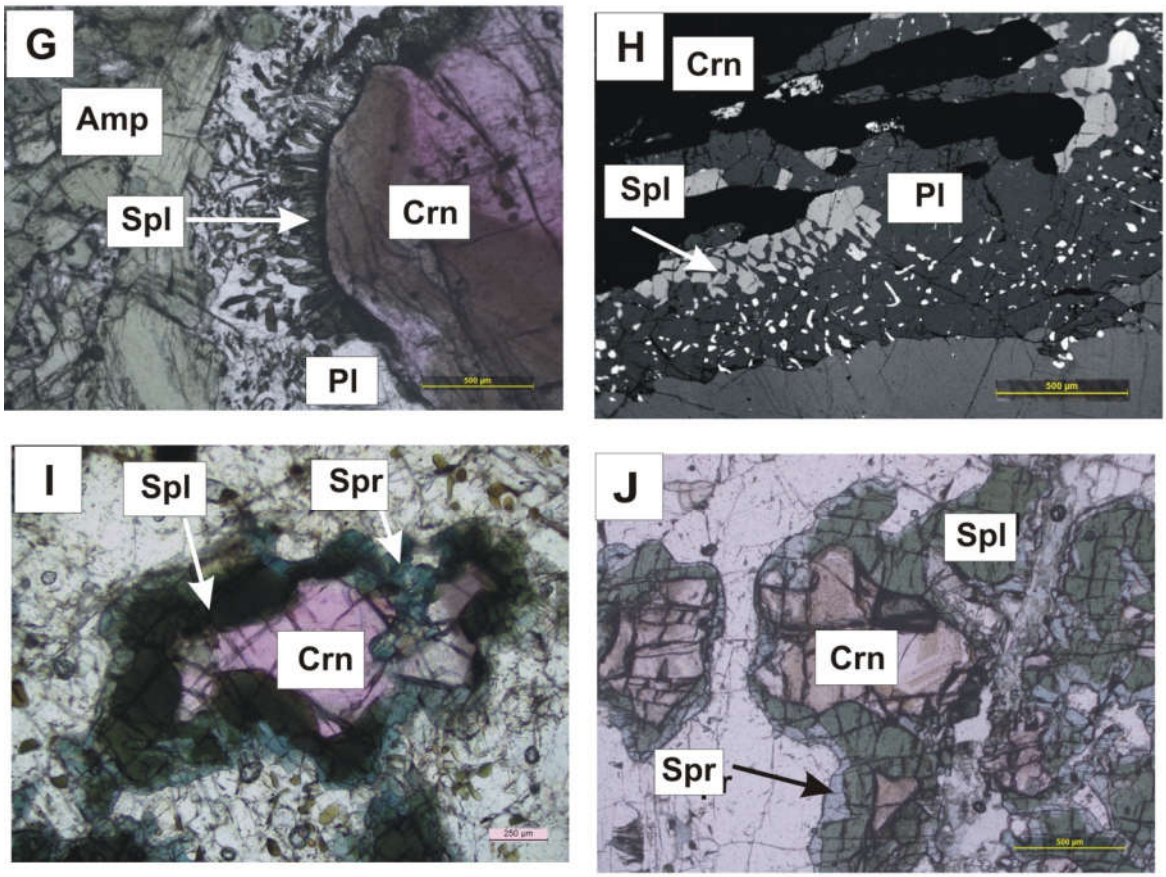

Fig 3.(G) PPL image and (H) BSE image are showing symplectite intergrowth of Spl+Pl formed between Amp and Crn. The proportion of Spl is decreasing from away from the Crn boundary. (I, J) Pink Crn is surrounded by double corona of Spl and Spr in the Pl+Amp matrix. (Mineral abbreviation Evans et al 2010).

1. Corundum forms at the expense of plagioclase;

2. Corundum reacts with matrix amphibole to form spinel + plagioclase i.e. corona or symplectite depending upon contrasting diffusion of components. In dominantly solid-state processes, where rate of diffusion of components is not very fast, product phases can form symplectite or compound coronae depending upon the reaction kinetics (reviewed in Vernon 2004). Observations from aluminous granulites suggest that a product phase, which is richer in Al (e.g., sillimanite), tends to grow proximal to the Al-rich reactant phase (e.g., spinel), whereas other product phase(s) form the outer corona (Kelsey 2008; Harley 2008; White and Powell 2011; Karmakar and Schenk 2015, 2016). This has been explained by sluggish mobility of Al with respect to other components (such as Fe, Mg etc.), as is the case here.

3. Sapphirine preferentially replaces spinel, but the involvement of corundum in sapphirine formation cannot be ascertained from petrography alone.

(Mineral abbreviations Evans et.al 2010)

5. Mineral Chemistry:

Chemical compositions of the minerals were determined with a CAMECA CAMEBAX MICROBEAM electron microprobe at the University of Bonn, Germany. The instrument was operated at 15 kV accelerating voltage, 2 μm beam diameter, and 15 nA current. Natural mineral standards were used, and the raw data were corrected by PAP procedure (Pouchou and Pichoir 1984). Representative mineral compositions are presented in Table-1 a, b,c, (Appendix I) and Fig. 4(a,b,c).

Corundum:

The corundum contains Al^{3+}- 1.97-2.00 apfu and very low Fe^{3+}(0.01 apfu) and Cr^{3+} (0.02 apfu). (Table 1b)

Plagioclase:

The plagioclase is mainly anorthite with composition range An_{95}-An_{99}(Table-1b). It contains Si^{4+}- 2.02-2.08 apfu, Al^{3+}- 1.81-1.96 apfu, Ca^{2+}- 0.96-1.04 apfu and Na^{+}- 0.01-0.06 apfu. Plagioclase of the SLC records the most calcic compositions ever recorded worldwide.

Spinel:

The general formula of normal spinel is AB_2O_4 where A is the tetrahedral site contains Mg^{2+}- 0.58-0.68 apfu, Fe^{2+}- 0.31- 041 apfu and the X_{Mg}=0.62-0.65 (Table-1c). B is the octahedral site contains Al^{3+} 1.92-1.96 apfu, Fe^{3+} 0.04-0.08 apfu and very little Cr^{3+} 0.001 apfu. Thus compositionally it is highly Al, Mg rich spinel.

Sapphirine:

The sapphirine contains Si^{4+} 1.35-1.52 apfu, Al^{3+} 8.83-9.10 apfu, Cr^{3+} 0.01-0.02 apfu, Fe^{3+} 0.51-0.58 apfu and Mg^{2+} 3.05- 3.14 apfu. The X_{Mg} is 0.84-0.86 (Table-1c). The compositions of the sapphirine areplotted in the binary diagram Al+Cr vs. Si+Mg+Fe (Fig. 4c) where they plot close to the 7:9:3 end member, indicating that they are peraluminous.

Clinozoesite:

Clinozoesite contains Si^{4+} 2.98-3.01 apfu, Al^{3+} 2.77-2.82 apfu, Fe^{3+} 0.11-0.17 apfu, Ca^{2+} 2.07-2.08 apfu with low Mg^{2+} (0.01 apfu).

Amphibole:

Amphiboles has general formula $AB_2C_5T_8O_{22}(OH)_2$ where A=Na, K, Ca, Li, B= Na, Li, Ca, Mn, Ti, Fe^{3+}, T=Si, Al, Ti. Primary classification of amphibole is done by the basis of B cation. The amphibole has X_{Mg}=0.89, ^{B}(Mg+Fe+Mn+Li)= 0.10-0.15 (<0.5), ^{B}(Ca+Na)= 1.83-1.89 (>1.5, Table-1a). Thus according to the classification scheme of Leake et al. 1997 the amphiboles fall in calcic group, and straddle the boundary between Ca-Pargasite and Ca-Tschemakite(Fig. 4a,b). The amphiboles are highly magnesian and aluminous.

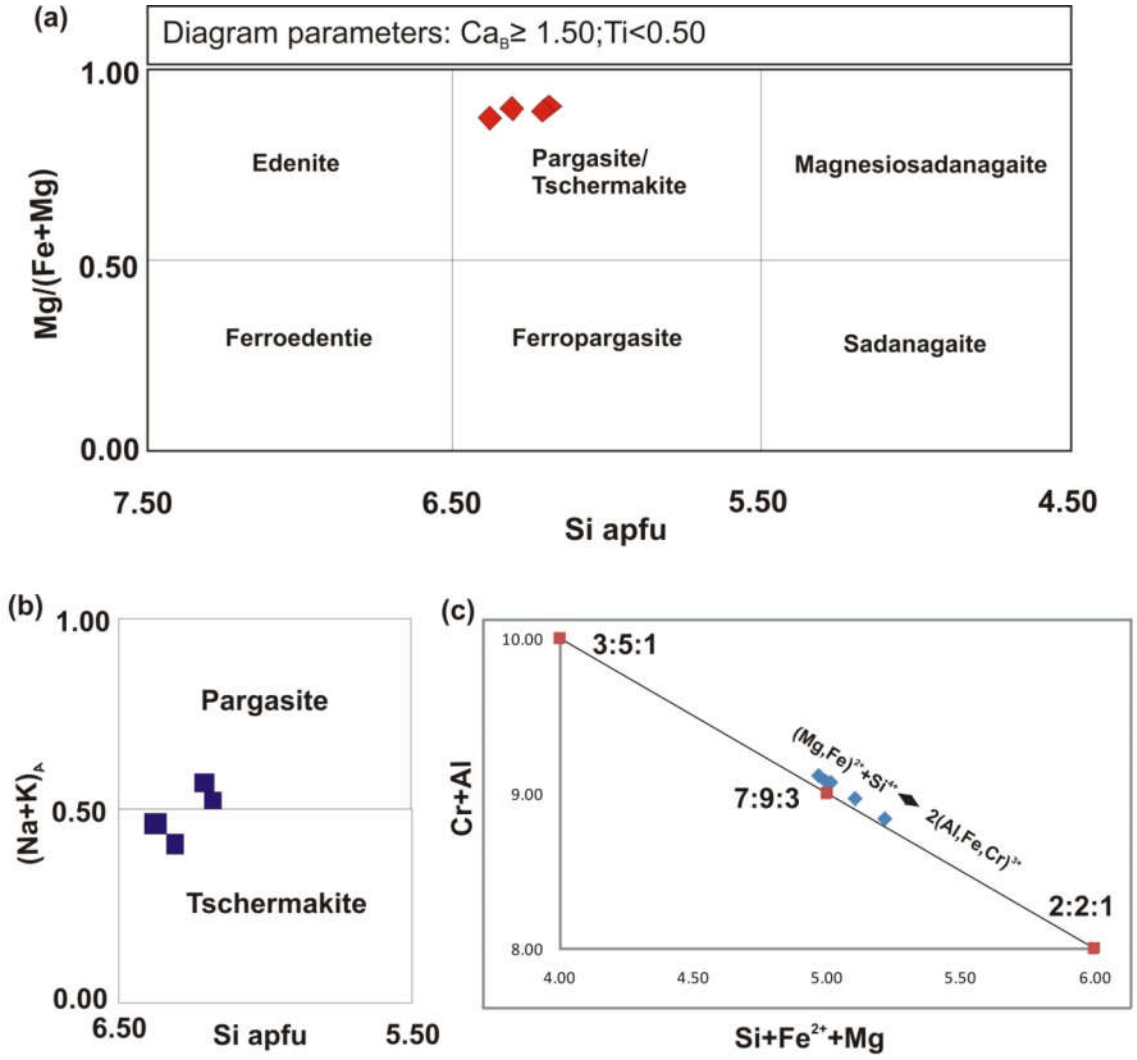

Fig 4.(a) Mg/(Mg+Fe^{2+}) vs. Si (apfu) plot and (b) $(Na+K)_A$ vs. Si (apfu) after Leake et al. 1997, showing amphibole compositions plot in the field of pargasite and tschermakite. (c) Cr+Al vs. Si+Fe^{2+}+Mg plot showing sapphirine compositions plot close to the 7:9:3 end member.

6. Textural modeling using CSpace:

Principle of CSpace:

The law of conservation of mass states that the total mass of all substances present before and after a chemical reaction remains the same. That is, atoms are neither created nor destroyed in chemical reaction, so the chemical equations must be balanced. If there are *m* numbers of linear equations connecting *n* number of independent variables then the equations can be written as,

$$
\begin{array}{c}
a_{11}X_1 + a_{12}X_2 + a_{13}X_3 + \ldots + a_{1n}X_n = Y_1 \\
a_{21}X_1 + a_{22}X_2 + a_{23}X_3 + \ldots + a_{2n}X_n = Y_2 \\
a_{31}X_1 + a_{32}X_2 + a_{33}X_3 + \ldots + a_{3n}X_n = Y_3 \\
\ldots\ldots\ldots\ldots\ldots\ldots\ldots\ldots\ldots\ldots\ldots\ldots \\
a_{m1}X_1 + a_{r2}X_2 + a_{r3}X_3 + \ldots + a_{mn}X_n = Y_m
\end{array}
$$

This can be written in the matrix form as, A.X= Y,…….(1)

$$
\begin{pmatrix} a11 & a12 & a13 & \ldots & a1n \\ a21 & a22 & a23 & \ldots & a2n \\ \ldots & \ldots & \ldots & \ldots & \ldots \\ am1 & am2 & am3 & & amn \end{pmatrix} . \begin{pmatrix} X1 \\ X2 \\ \ldots \\ Xn \end{pmatrix} = \begin{pmatrix} Y1 \\ Y2 \\ \ldots \\ Yn \end{pmatrix}
$$

Where A is an *m* by *n* matrix, describing the *m* number of phases with *n* number of system components. There exists a number of techniques e.g. Gauss Jordon elimination, SVD etc. to solve the equation (1) (Press et al. 1989).C-Space uses singular value decomposition (SVD), which was first introduced to petrologic applications by Fisher (1989; see this paper for a discussion of the relative merits of SVD with regard to other algebraic techniques).SVD encompasses a most useful family of methods in linear algebra which derives from a theorem that states that any m by n matrix A (m >=n) can be written as the product of an *m* by *r* column-orthogonal matrix U, and *r* by *r* diagonal matrix Σ with positive or zero elements, and the transpose of an *n* by *r* orthogonal matrix V:

$$\mathbf{A = U\, \Sigma\, V^t}$$

The usefulness of SVD derives from several of its fundamental properties. The SVD of a matrix can always be obtained, whether it is singular or not, and is almost unique (up to same permutations of columns of U, Σ and V, or linear combinations of U and V columns with equal corresponding elements of Σ). Both U and V are orthogonal, so their inverse is simply their transpose (i.e., $U^tU= V^tV=I$, the identity matrix). The number of non-zero diagonal elements of Σ (called singular values) gives the rank of A, whereas U and V each contain a set of independent vectors (also called ``orthonormal basis'') that fully characterize the range and null space of A, respectively. Of particular interest is that the columns of V whose same-numbered elements of Σ are zero form an orthonormal basis for the null space, thus directly giving coefficients for any linear dependencies in A. These, or any linear combination thereof, fully represent the range of linear relations (such as reactions or mass-balances) implicit in a matrix of compositions. A major advantage of SVD is that it allows robust handling of linear systems of equations such as Eq. (1) because of its ability to diagnose problems when the matrix of compositions A is nearly singular through simple inspection of its singular values. The mathematics and computation of SVD are discussed by, e.g., Golub and Van Loan (1983) and Press et al. (1989).

Now *m* numbers of phases are taken in the rows and *n* numbers of components are taken in the columns in the C-Space data window to generate *m* by *n* matrix of A. The Matrix Analyze Wizard (MAW) helps to derive every possible reaction based on the phase component relationships. Out of the possible balanced reactions, only those which can explain the observed textural and relations between the phases, are considered, i.e., reactants and the product phases must lie on the opposite side of the reaction and the calculated and the observed proportions of the product minerals must tally within a few vol%.C-Space's graph window is also helpful of generating triangular and 3D single and stereoscopic tetrahedral barycentric plots where tieline flip reactions and compositions of different minerals has been plotted. The C-Space program, which is based on the algorithm published by Fisher (1989, 1993), is therefore, an elegant tool to model reaction textures that may help decipher the physico-chemical conditions, which a given rock might have evolved through (Lang et al. 2004, Sengupta et al. 2009).

The molar volumes of the minerals that are used in this study are calculated at 7 kbar, 750 °C, the mean pressure–temperature estimated for the SLC. The updated thermodynamic data of Holland and Powell (1998) and the computer program of PERPLEX_6.6.8 (Connolly

2005, 2009) are used to obtain the molar volume data. For solid-solution minerals, the molar volume (V_{SS}) is calculated from the following relation:

$V_{SS} = (X_A \times V_A) + (X_B \times V_B)$,

where A and B are the end members of the solid-solution phase N, X is the mole fraction of the corresponding end member, and V is the molar volume of that end member.

***Application and discussion*:**

The C-Space program has been used to balanced chemical reactions using mineral compositions in Sample-160.

In order to balance the textural reaction:

Crn + Amp → Pl + Spl,

the phases considered are Crn, Amp, Spl, Pl and Spr. The components considered Si, Mg, Fe^{2+}, Al, Na, K and Ca. Since Amp is the only hydrous mineral containing K (and Na), H_2O, Na, K are considered as mobile components. Since spinel and amphibole have different X_{Mg} values,(X_{Mg}^{spl}= 0.68, X_{Mg}^{amp}= 0.89)SiO_2 aqueous and Mg (or Fe)are also considered as mobile components. Using C-Space,the following balanced reaction is obtained for formation of spl+pl symplectite:

R1: **100.92 Crn + 33.02 Amp = 60.97 Pl + 90.15 Spl + 33.88 H_2O + 18.58 Na^+ + 1.00 K^+ + 88.41 SiO_2(aqueous) + 51.11 Mg^{2+} (coefficients are given up to second decimal).**

Volume ratio: **An:Spl = 1.7:1**.

The calculated mass balanced reaction predicts the volume of the product spinel will be lower than the volume of the anorthite, which is in good agreement with the petrographic observations. It is also evident from reaction (1) that a number of chemical species including aq.SiO_2, Na^+, Mg^{2+}, and Fe^{2+} became mobile during the development of the coronitic spinel and anorthite.

Now, it has been mentioned previously that sapphirine preferentially replaces spinel, but the involvement of corundum in sapphirine formation cannot be ascertained from

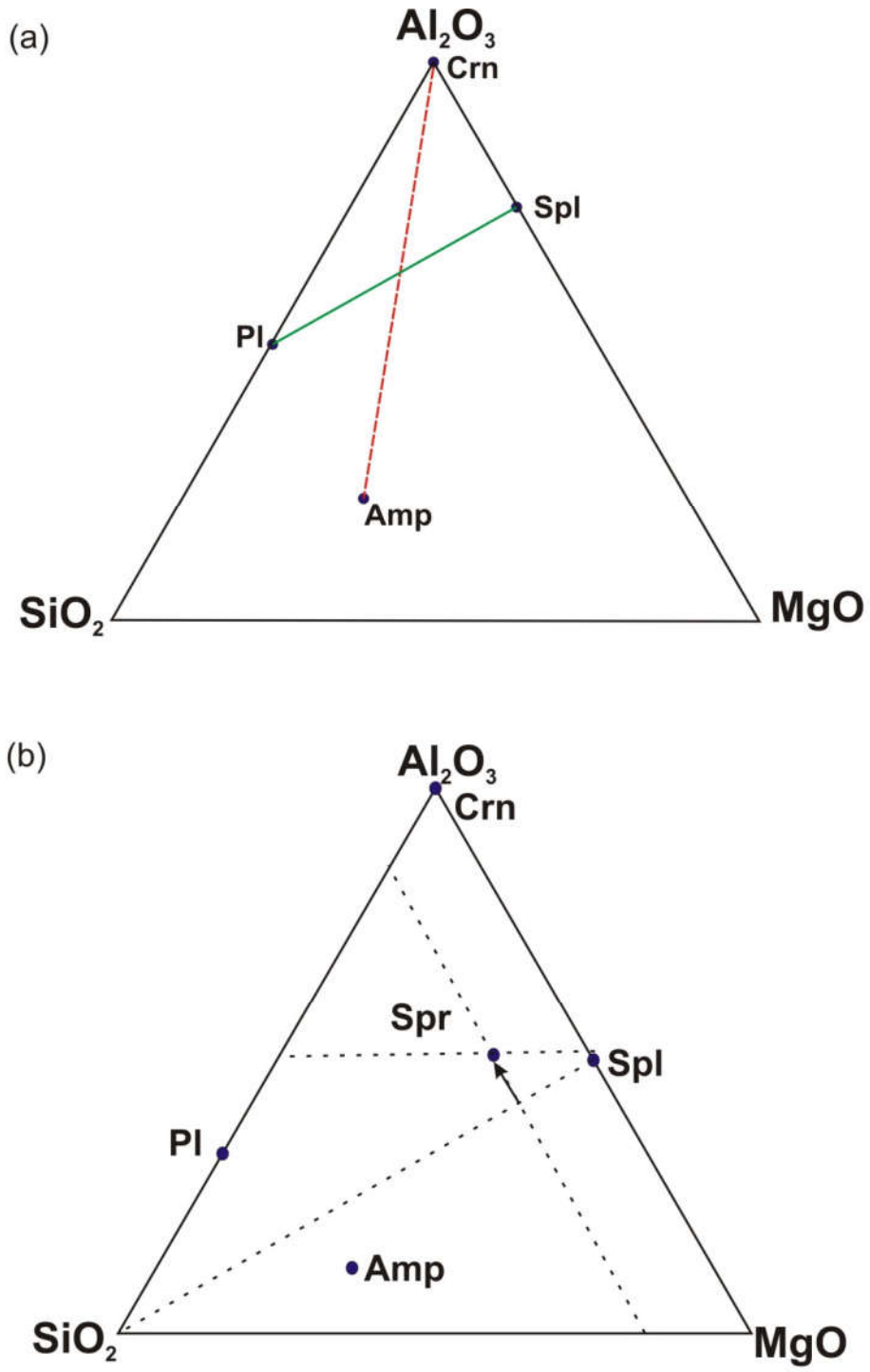

Fig 5. SiO_2-Al_2O_3-MgO ternary diagrams showing: (a) tieline flip reaction Crn+Amp⟶Pl+Spl (B)Compositions of the mineral assemblages.

petrography alone. Accordingly, phase relations in the system Al_2O_3–SiO_2–MgO (Fig. 5 a,b) were constructed, which indicate that minerals that developed prior to sapphirine (i.e., anorthite + spinel + amphibole) cannot develop sapphirine in an isochemical process. The dominant occurrence of sapphirine (Mg–Al–silicate) around spinel (Mg–Al oxide) indicates that spinel was certainly one of the reactants. Sapphirine in the studied rocks is peraluminous in composition (Fig. 4c). Therefore, transformation of spinel to sapphirine requires a source for Al_2O_3 and also SiO_2 (Fig.5 a,b). Most natural sapphirine compositions are less aluminous than the 7:9:3 end member and plot closer to the 2:2:1 end member (reviewed in Taylor-Jones and Powell 2010; Shazia et al. 2012). In the few reported occurrences of peraluminous sapphirine from a variety of rock types, sapphirine was always found to co-exist with or replace an aluminous phase such as corundum, kyanite, or sillimanite (Higgins et al. 1979; Sutherlandand Coenraads 1996; Tenthorey et al. 1996; Raith et al. 1997; Godard and Mabit 1998; Baba 2003; Tsunogae and Santosh 2005; Suman et al. 2006; Raith et al. 2008; Berger et al. 2010; Kruckenberg and Whitney 2011; Guo et al. 2012; Karmakar and Schenk 2015). Accordingly, corundum has been considered as the other reactant phase together with spinel, as is also supported by phase relations in Fig. 5a,b. Textural modeling identifies the following mass balanced reaction for sapphirine formation:

R2: **2.06 Crn + 2.65 Spl + 1.55 SiO_2 (aqueous) + 1.25 Mg^{2+} = 1.00 Spr (Coefficients are presented in second decimal)**

ΔV solid = +3.92

In complex natural systems, it is quite likely that the construed reaction (2) is linked to some other reactions occurring in adjoining domains. Here, only the net sapphirine forming reaction is presented. Reaction (2) predicts that significant amounts of SiO_2 and Mg^{2+} are to be brought to the site of spinel ± corundum for progress of the reaction. Since the studied rocks do not contain any free source of SiO_2 or Mg^{2+}, these components can only be supplied by infiltrating fluids. It is, therefore, presumed that the narrow zones where sapphirine concentrated were the conduits of the infiltrating fluids. Reaction (2) has a large positive volume change. This follows that the sapphirine forming reaction (reaction 2) would destroy the porosity and permeability of the rocks and hinder the flow of fluid. This may explain, at least partly, the low volume of sapphirine. The fact that sapphirine is restricted to certain zones, whereas adjoining spinel-bearing domains are devoid of sapphirine, suggests

that fluid–mineral interaction exerted greater influence than the ambient physical condition of metamorphism (Raith et al. 2008, Berger et al. 2010).

7. P-T Condition of metamorphism:

Schreinemakers rules for construction of P-T grid:

Before looking into the petrogenetic grids, let's first address a few simple rules that govern the way reactions behave when they intersect on phase diagrams. "Topology" may also be used to describe such geometric patterns of univariant reaction curves. The rules follow the strictly geometric treatment of **Schreinemakers** (see Zen, 1966, for a complete description of the method, or Powell, 1991, for some practical examples). Although initially applied to *T-P* phase diagrams, the method is general and can be applied to *T-X* diagrams, or activity–activity diagrams, or any other diagram involving two intensive variables. We shall use *T-P* diagrams for our rock samples. The Schreinemakers rules state that:

1. When P=C+2 an invariant point results where P= number of phases, C= number of components.

2. C+2 univariant reaction curves must emanate from each invariant point.

3. If two reactions have fewer than C no. of phases in common, they cross in an **indifferent** fashion: they are independent of each other and do not require an invariant point at the intersection.

4. If, on the other hand, two intersecting univariant reactions have *C* phases in common, their intersection cannot be indifferent, and the intersection generates an invariant point, plus other univariant curves emanating from it, as described in rules 1 and 2 above. This is so because each univariant curve must have phases at equilibrium, and one of the phases cannot be the same for each intersecting curve (otherwise, they would be the same curve). Thus phases coexist at the intersection of the curves, and this implies an invariant situation.

5. The metastable extensions of each of these reactions will thus lie on the side of the first reaction in which the absent-phase is stable.

6. It follows from rule 5 that if two reactions that meet at an invariant point are known and can be located and oriented fairly accurately on a phase diagram, the full topology of the invariant point can be deduced.

7. It also follows from rule 5 that any divariant field cannot occupy a sector >180^{o} about any invariant point. Otherwise, the metastable extension would extend into the field in which the phase is unstable.

Application of Screinemaker's principles :

To understand the PT stability of the peraluminous assemblages in the studied rocks of the SLC, partial reaction grids have been developed in the systems CASH ($CaO–Al_2O_3–SiO_2–H_2O$), CMASH ($CaO–MgO–Al_2O_3–SiO_2–H_2O$) and NCMASH ($Na_2O–CaO–MgO–Al_2O_3–SiO_2–H_2O$) using the computer program PERPLEX_6.6.8 (Connolly 2005, 2009) and the updated thermodynamic data set of Holland and Powell (1998).The univariant reactions in Fig. 6 are adjusted for activities of the solid-solution phases, calculated from the measured compositions of the phases with the program AX (Holland and Powell 2003, 2015): clinozoisite = 0.86; anorthite = 0.96; albite = 0.10; tschermakite = 0.01; pargasite = 08; spinel = 0.65. Activity corrected phases are denoted with a (*). Because of their absence, the activity of the remaining phases has been considered as unity. Only the reactions relevant for the present study have been discussed.

CASH (CaO -Al_2O_3- SiO_2- H_2O system):

In the PT diagram (Fig 6) there is one invariant point (I_1) where the phases margarite, corundum, kyanite , anorthite (an*) and clinozoesite (czo *) are stable. The invariant point is at P=10.8 kbar, T=710^{o}C. The univariant reactions bounding the margarite stability field are:

Mrg→Crn+An* (1)

Mrg →Ky+ Czo*+ Crn (2)

The stability field of kyanite (+ clinozoisite) is marked by reaction (2) and:

Czo* + Ky → An* + Crn (3)

Reaction (3) also marks the first appearance of corundum, which coexists with anorthite.

Czo* → Grs + An* + Crn (4)

Reaction (4) marks the appearance of grossular coexisting with corundum. However, as both kyanite and grossular are absent in the studied rocks, from the CASH grid, the P-T conditions of the observed assemblage Crn + An* is delineated between reactions 2, 3 and 4. This bi-variant field is stable over a large range of P and T.

CMASH ($CaO – MgO - Al_2O_3 - SiO_2 - H_2O$ system):

From textural observations and modeling,it is clear that spinel forms due to reaction of corundum and amphibole. This is represented by the following CMASH reaction:

Crn + Czo* + Ts* → Spl* + An* (5)

This reaction represents the appearance of spinel and anorthite in the rock.

The following reaction constrains the high temperature stability limit of corundum + amphibole:

Spl* + Czo* → Grs + Crn + Ts* (6).

NCMASH ($Na_2O - CaO – MgO - Al_2O_3 - SiO_2 - H_2O$ system):

The following NCMASH reaction constrains the lower P stability limit of corundum + amphibole:

Ab* + Ts* + Czo* + Crn → Parg* + An* (7)

Reactions 5 and 7 thus indicate that spinel formed due to corundum breakdown during decompression.

Dispositions of several reaction lines thus constrain the assemblage corundum + amphibole + anorthite ± clinozoisite to lie within 11 ± 2 kbar and ~750 ± 50 °C (Fig. 6). The inferred P–T values are in good agreement with the quantitative P–T values obtained from adjacent mafic granulites, 11–12 kbar, 700–800 °C (Talukdar 2016), both of which share the same

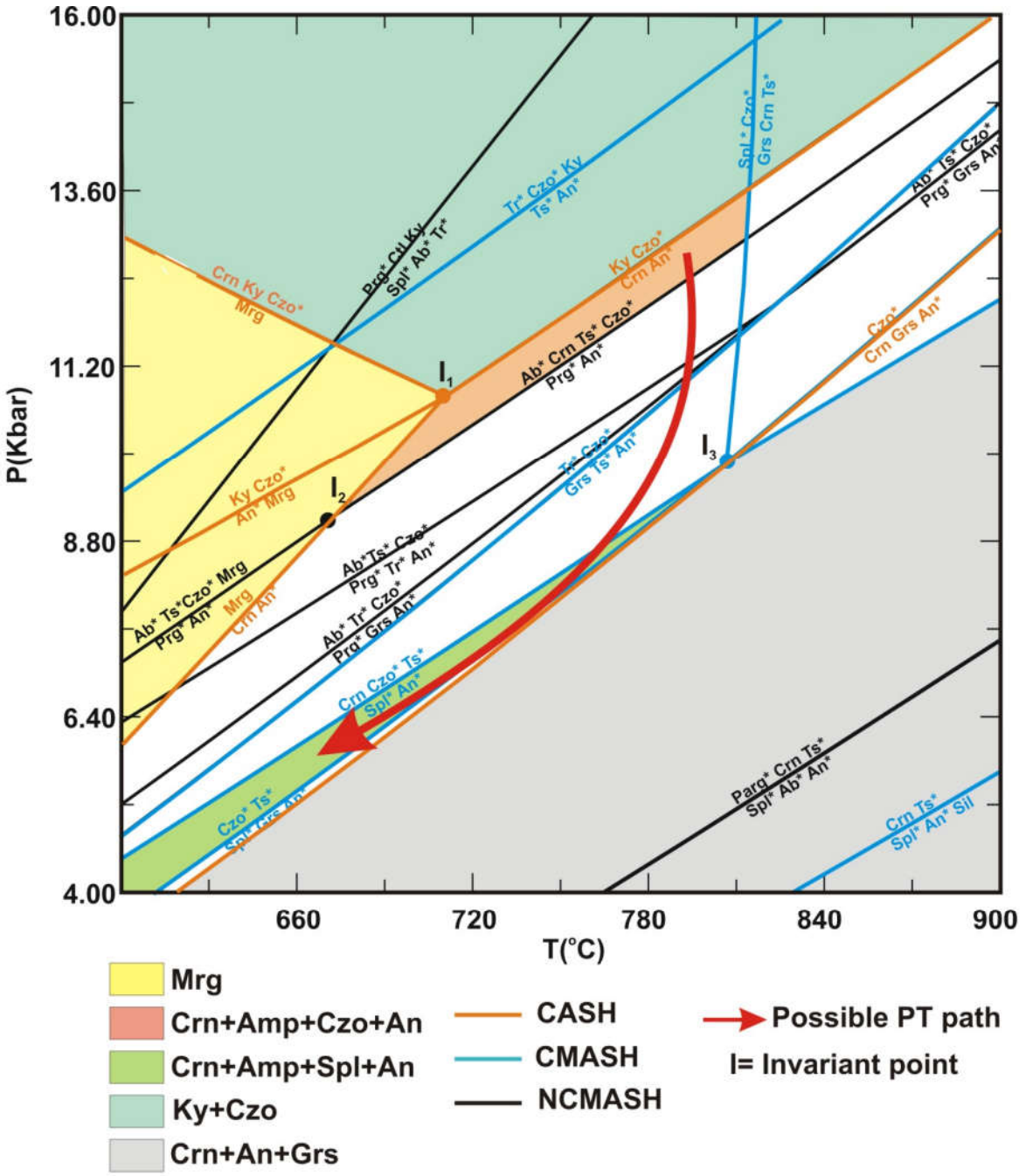

Fig 6. Activity constrained partial petrogenetic grids in the CaO-Al_2O_3-SiO_2-H_2O(CASH)-CaO-MgO-Al_2O_3-SiO_2-H_2O (CMASH)-Na_2O-CaO-MgO-Al_2O_3-SiO_2-H_2O(NCMASH) system. X* activity constrained phase, X pure phase. The stability field of different mineral assemblages are shown in colours. The red arrow represents the possible decompressive PT path.

deformation and metamorphic history. These metamorphic P–T conditions indicate that the magmatic protoliths of the SLC, which is presumed to be a fragment of Archean oceanic crust, were buried to a depth of more than 30 km, where infiltration-driven metamorphism produced amphibole ± corundum.

8. Discussion:

At the peak metamorphic condition the stable assemblage is anorthite + amphibole + corundum ± clinozoisite . Though textural relations predict that corundum most likely formed at the expense of anorthite, it is not possible to predict here the mechanism of corundum formation. The opinion varies from magmatic crystallization at high-pressure (Sen and Presnall 1984; Liu and Presnall 1990) to UHP metamorphism at mantle depth (Morishita and Kodera 1998; Morishita 2004) to crustal anatexis of anorthosite (Kullerud et al. 2012; Karmakar et al. 2017). But it is quite clear from textural relations that spinel + anorthite coronae formed after corundum. Topological constraints in parts of the NCMASH system suggest that the assemblage corundum + amphibole + anorthite + clinozoisite was stabilized during high-pressure metamorphism (11 ± 2 kbar, 750 ± 50 °C; Fig. 6). The estimated pressure corresponds to a burial of the SLC 32-40 km depth during metamorphism (1 kbar ~ 3.3 km) A steeply decompressive P–T path developed coronitic spinel + anorthite at the expense of corundum + amphibole in an open system at 7–8 kbar and ~700°C (Fig. 6). The decompression exhumed the lower crust between 22-26 km. That means an exhumation of >14 km. Volumetrically minor sapphirine developed after spinel, also along the decompressive P–T path, due to Mg-Si metasomatism in the presence of aqueous fluid(s) that permeated the rock. The Mg and Si needed for sapphirine formation from corundum and spinel was most likely released during the spinel formation, through extremely channelized fluid flow along the grain boundaries.

Acknowledgements

I would like to thank Prof. Pulak Sengupta, Dept. of Geological Sciences, Jadavpur University and Dr. Shreya Karmakar, Post-doctoral research fellow, Dept. of Geological Sciences, Jadavpur University for supporting me throughout my dissertation work. Finally, I thank to my senior lab members and my friends for providing valuable opinion on several aspects of this work.

Appendix I

Table 1a. Representative electronmicroprobe analyses of amphibole

Sample	S-160	S-160	S-140	S-140
No.	64*	80	100	131
SiO_2	43.52	43.73	45.24	43.94
TiO_2	0.05	0.04	0.21	0.22
Al_2O_3	15.73	16.00	15.21	15.16
Cr_2O_3	0.05	0.17	0.02	0.06
FeO	7.54	7.42	6.96	7.04
MnO	0.15	0.11	0.09	0.10
MgO	15.93	16.07	15.91	15.82
CaO	11.12	11.42	11.57	11.21
Na_2O	2.43	2.21	2.19	1.89
K_2O	0.16	0.13	0.06	0.06
Total	96.68	97.30	97.46	95.50
Oxygen (pfu)	23	23	23	23
Classification and nomenclature after Leake et al. (1997, 2004)				
Si	6.21	6.19	6.38	6.31
Al (IV)	1.79	1.81	1.62	1.17
Ti	0.00	0.00	0.00	0.00
Sum T	8.00	8.00	8.00	8.00
Al (VI)	0.85	0.85	0.91	0.88
Ti	0.01	0.00	0.02	0.02
Cr^{+3}	0.01	0.02	0.00	0.01
Fe^{+3}	0.49	0.53	0.36	0.46
Mg	3.39	3.39	3.34	3.39
Fe^{+2}	0.26	0.21	0.37	0.24
Mn	0.00	0.00	0.00	0.00
Li	0.00	0.00	0.00	0.00
Sum C	5.00	5.00	5.00	5.00
Mg	0.00	0.00	0.00	0.00
Fe^{+2}	0.15	0.14	0.09	0.14
Mn	0.02	0.01	0.01	0.01
Li	0.00	0.00	0.00	0.00
Ca	1.70	1.73	1.75	1.73
Na	0.13	0.11	0.15	0.12
Sum B	2.00	2.00	2.00	2.00
Ca	0.00	0.00	0.00	0.00
Na	0.54	0.49	0.45	0.40
K	0.03	0.02	0.01	0.01
Sum A	0.57	0.52	0.46	0.42
TOTAL	15.57	15.52	15.46	15.42
	Ca-Par	**Ca-Par**	**Ca-Tsk**	**Ca-Tsk**

Table 1b. Representative electronmicroprobe analyses of plagioclase and corundum

Sample	S-160	S-160	S-160	S-140	S-140	S-160	S-160	S-140	S-140
Mineral	Pl	Pl	Pl	Pl	Pl	Crn	Crn	Crn	Crn
No.	61*	78	93	154	144	68*	22	163	24
SiO_2	43.34	43.34	43.39	43.82	44.96	0.00	0.00	0.00	0.02
TiO_2	0.00	0.00	0.01	0.01	0.01	0.02	0.00	0.01	0.00
Al_2O_3	35.49	35.72	35.22	34.81	34.62	99.23	99.71	98.10	98.02
Cr_2O_3	0.00	0.00	0.00	0.00	0.00	0.06	0.00	1.66	1.52
Fe_2O_3	-	-	-	-	-	0.54	0.39	0.18	0.45
FeO	0.11	0.10	0.12	0.09	0.04	0.00	0.00	0.00	0.02
MnO	0.00	0.00	0.01	0.00	0.00	0.02	0.00	0.03	0.00
MgO	0.00	0.02	0.00	0.00	0.00	0.00	0.00	0.00	0.02
CaO	19.27	19.78	19.08	20.88	19.96	0.00	0.00	0.00	0.01
Na_2O	0.57	0.58	0.64	0.16	0.32	0.00	0.00	0.01	0.00
K_2O	0.00	0.01	0.00	0.01	0.00	0.00	0.00	0.01	0.02
Total	98.78	99.54	98.47	99.77	99.91	99.87	100.13	100.00	100.06
Oxygen (pfu)	8	8	8	8	8	3	3	3	3
Si	2.03	2.02	2.04	2.04	2.08	0.00	0.00	0.00	0.00
Ti	0.00	0.00	0.00	0.00	0.00	0.00	0.00	0.00	0.00
Al	1.96	1.96	1.95	1.91	1.89	1.99	2.00	1.97	1.97
Cr	0.00	0.00	0.00	0.00	0.00	0.00	0.00	0.02	0.02
Fe3+	0.00	0.00	0.00	0.00	0.00	0.01	0.00	0.00	0.01
Fe2+	0.00	0.00	0.00	0.00	0.00	0.00	0.00	0.00	0.00
Mn	0.00	0.00	0.00	0.00	0.00	0.00	0.00	0.00	0.00
Mg	0.00	0.00	0.00	0.00	0.00	0.00	0.00	0.00	0.00
Ca	0.97	0.99	0.96	1.04	0.99	0.00	0.00	0.00	0.00
Na	0.05	0.05	0.06	0.01	0.03	0.00	0.00	0.00	0.00
K	0.00	0.00	0.00	0.00	0.00	0.00	0.00	0.00	0.00
Total	5.01	5.03	5.01	5.01	4.99	2.00	2.00	2.00	2.00
Xan	0.95	0.95	0.94	0.99	0.97				

Table 1c. Representative electronmicroprobe analyses of spinel, sapphirine and clinozoisite

Sample	S-160	S-160	S-160	S-140	S-140	S-160	S-160	S-160	S-140	S-140		
Mineral	Spl	Spl	Spl	Spl	Spl	Spr	Spr	Spr	Spr	Spr	Czo	Czo
No.	51*	58	3	120	121	59*	83	24	96	90	67	69
SiO_2	0.01	0.00	0.00	0.00	0.03	11.64	11.50	11.38	12.83	12.11	39.21	38.60
TiO_2	0.00	0.02	0.00	0.00	0.01	0.00	0.01	0.00	0.02	0.00	0.00	0.00
Al_2O_3	63.01	63.58	65.13	61.57	61.93	64.85	64.70	65.04	63.10	63.89	31.20	30.44
Cr_2O_3	0.06	0.09	0.08	0.07	0.06	0.09	0.04	0.19	0.05	0.01	0.00	0.18
Fe_2O_3	4.02	3.87	1.99	3.76	3.33						1.92	2.97
FeO	14.66	14.66	16.68	18.44	18.57	5.71	5.67	5.12	5.88	5.29	0.00	0.00
MnO	0.09	0.13	0.07	0.17	0.12	0.05	0.00	0.03	0.03	0.04	0.10	0.00
MgO	17.65	17.79	16.85	14.66	14.86	17.24	17.38	17.59	17.56	17.67	0.03	0.05
ZnO	0.05	0.08	0.00	0.06	0.08						0.00	0.00
CaO	0.00	0.00	0.00	0.00	0.00	0.01	0.02	0.01	0.00	0.00	25.12	25.11
Na_2O	0.00	0.00	0.00	0.05	0.00	0.00	0.02	0.00	0.00	0.03	0.01	0.08
K_2O	0.00	0.01	0.01	0.00	0.00	0.00	0.00	0.00	0.00	0.00	0.02	0.00
Total	99.56	100.23	100.80	98.79	98.98	99.59	99.34	99.37	99.48	99.04	97.61	97.43
Oxygen (pfu)	4	4	4	4	4	20	20	20	20	20	12.5	12.5
Si	0.00	0.00	0.00	0.00	0.00	1.38	1.37	1.35	1.52	1.44	3.01	2.98
Ti	0.00	0.00	0.00	0.00	0.00	0.00	0.00	0.00	0.00	0.00	0.00	0.00
Al	1.92	1.92	1.96	1.93	1.93	9.07	9.07	9.10	8.83	8.96	2.82	2.77
Cr	0.00	0.00	0.00	0.00	0.00	0.01	0.00	0.02	0.00	0.00	0.00	0.01
Fe^{3+}	0.08	0.07	0.04	0.08	0.07	0.00	0.00	0.00	0.00	0.00	0.11	0.17
Fe^{2+}	0.32	0.31	0.36	0.41	0.41	0.57	0.56	0.51	0.58	0.53	0.00	0.00
Mn	0.00	0.00	0.00	0.00	0.00	0.00	0.00	0.00	0.00	0.00	0.01	0.00
Mg	0.68	0.68	0.64	0.58	0.59	3.05	3.08	3.11	3.11	3.14	0.00	0.01
Zn	0.00	0.00	0.00	0.00	0.00	0.00	0.00	0.00	0.00	0.00	0.00	0.00
Ca	0.00	0.00	0.00	0.00	0.00	0.00	0.00	0.00	0.00	0.00	2.07	2.08
Na	0.00	0.00	0.00	0.00	0.00	0.00	0.00	0.00	0.00	0.01	0.00	0.01
K	0.00	0.00	0.00	0.00	0.00	0.00	0.00	0.00	0.00	0.00	0.00	0.00
Total	3.00	3.00	3.00	3.00	3.00	14.08	14.10	14.09	14.06	14.08	8.02	8.04
X_{Mg}	0.68	0.68	0.64	0.59	0.59	0.84	0.85	0.86	0.84	0.86		

References:

1. Berger, J., Féménias, O.,Ohnenstetter, D., Plissart, G., and Mercier, J.-C.C. (2010) Origin and tectonic significance of corundum–kyanite–sapphirine amphibolites from the Variscan French Massif Central. Journal of Metamorphic Geology, 28, 341–360.
2. Bhaskar Rao, Y.J., Chetty, T.R.K., Janardhan, A.S., and Gopalan, K. (1996) Sm–Nd and Rb–Sr ages and *P–T* history of the Archaean Sittampundi and Bhavani layered meta anorthosite complexes in Cauvery Shear Zone, South India: Evidence for Late Proterozoic reworking of Archean crust. Contributions to Mineralogy and Petrology, 125, 237–250.
3. Braun, I., and Kriegsman, L.M. (2003) Proterozoic crustal evolution of southernmost India and Sri Lanka. In M. Yoshida, B.F. Windley, and S. Dasgupta, Eds., Proterozoic East Gondwana: Supercontinent Assembly and Breakup, 206, 169–202. Geological Society of London, Special Publications.
4. Chetty, T.R.K. (1996) Proterozoic shear zones in southern granulite terrain, India. In M. Santosh and M. Yoshida, Eds., The Archaean and Proterozoic Terrains in Southern India within East Gondwana, 3, 77–89. Gondwana Research Group Memoir, International Association for Gondwana Research, Trivandrum, India.
5. Clark, C., Collins, A.S., Timms, N.E., Kinny, P.D., Chetty, T.R.K., and Santosh, M. (2009) SHRIMP U–Pb age constraints on magmatism and high-grade metamorphism in the Salem Block, southern India. Gondwana Research, 16, 27–36.
6. Connolly, J. (2005). Computation of phase equilibria by linear programming: a tool for geodynamic modeling and its application to subduction zone decarbonation. Earth and Planetary Science Letters, 236(1), 524–541.
7. Connolly, J. (2009). The geodynamic equation of state: What and how. Geochemistry Geophysics Geosystems, 10(10), 1–19.
8. Dutta, U., Bhui, U.K., Sengupta, P., Sanyal, S., and Mukhopadhyay, D. (2011) Magmatic and metamorphic imprints in 2.9 Ga chromitites from the Sittampundi layered complex, Tamil Nadu, India. Ore Geology Reviews, 40, 90–107.
9. Ghosh, J.G., De Wit, M.J., and Zartman, R.E. (2004) Age and tectonic evolution of Neoproterozoic ductile shear zones in the southern granulite terrain of India with implications for Gondwana studies. Tectonics, 23, 1–38.

10. Holland, T.J.B., and Powell, R. (1998) An internally consistent thermodynamic data set for phases of petrological interest. Journal of Metamorphic Geology, 16, 309–343 (updated online, 2002).——— (2000) AX, Mineral activity calculation for thermobarometry, computer program AX2 v. 2.2. Cambridge University, U.K.
11. Karmakar, S., Mukherjee, S., Sanyal, S., & Sengupta, P. (2017). Origin of peraluminous minerals (corundum, spinel, and sapphirine) in a highly calcic anorthosite from the Sittampundi Layered Complex, Tamil Nadu, India. Contributions to Mineralogy and Petrology, 172, 1–23. http://doi.org/10.1007/s00410-017-1383-8
12. Leake, B.E., Woolley, A.R., Birch, W.D., Burke, E.A.J., Ferraris, G., Grice, J.D., Hawthorne, F.C., Kisch, H.J., Krivovichev, V.G., Schumacher, J.C., Stephenson, N.C.N., and Whittaker, E.J.W. (2004) Nomenclature of amphiboles: Additions and revisions to the International Mineralogical Association's amphibole nomenclature. American Mineralogist, 89, 883–887.
13. Meissner, B., Deters, P., Srikantappa, C., and Kohler, H. (2002) Geological evolution of the Moyer, Bhavani and Palghat shear zones of southern India: Implications for Gondwana correlation. Precambrian Research, 114, 149–175.
14. Philpotts, A., and Ague, J. (2009) Principles of Igneous and Metamorphic Petrology, 2nd ed. Cambridge University Press, U.K.
15. Raith, M.M., Rakotondrazafy, R., and Sengupta, P. (2008) Petrology of corundumspinel-sapphirine-anorthite rocks (sakenites) from the type locality in southern Madagascar. Journal of Metamorphic Geology, 26, 647–667.
16. Raith, M.M., Srikantappa, C., Sengupta, P., Kooijman, E., and Upadhyay, D. (2010) Corundum–leucosome-bearing aluminous gneiss from Ayyarmalai, Southern Granulite Terrain, India: A textbook example of vapor phase-absent muscovite-melting in silica undersaturated aluminous rocks. American Mineralogist, 95, 897–907.
17. Ramadurai, S., Sankaran, M., Selvan, T.A., Windley, B.F., 1975. The stratigraphy and structure of the Sittampundi complex, Tamil Nadu, India. Journal of Geological Society of India 16, 409–414.
18. Saitoh, Y., Tsunogae, T., Santosh, M., Chetty, T.R.K., and Horie, K. (2011) Neoarchean high-pressure metamorphism from the northern margin of the Palghat-Cauvery suture zone, southern India: Petrology and zircon SHRIMP geochronology. Journal of Asian Earth Sciences, 42, 268–285.

19. Sengupta, P., Dutta, U., Bhui, U., and Mukhopadhyay, D. (2009a) Genesis of wollastonite- and grandite-rich skarns in a suite of marble–calc–silicate rocks from Sittampundi, Tamil Nadu: Constraints on the *P–T*–fluid regime in parts of the Pan-African mobile belt of South India. Mineralogy and Petrology, 95, 179–200.
20. Sengupta, P., Bhui, U.K., Braun, I., Dutta, U., and Mukhopadhyay, D. (2009b) Chemical substitutions, paragenetic relations and physical conditions of högbomite in Sittampundi layered anorthosite complex, south India. American Mineralogist, 94, 1520–1534.
21. Subramanium, A.P. (1956) Mineralogy and petrology of the Sittampundi complex, Salem district, Madras State, India. Geological Society of America Bulletin, 67, 317–390.
22. Srikantappa, C., Srinivas, G., Basavarajappa, H.T., Prakash Narasimha, K.N., asavalingu, B., 2003. Metamorphic evolution and fluid regime in the deep continental crust along the N–S Geotransect from Vellar to Dharapuram, Southern India. In: Ramakrishna, M. (Ed.), Tectonics of Southern Granulite Terrain: Geological Society of India Memoir, vol. 50, pp. 319–373.
23. Torres-Roldan, R.L., Garcia-Casco, A., and Garcia-Sanchez, P.A. (2000) C-Space: An integrated workplace for the graphical and algebraic analysis of phase assemblages on 32-bit wintel platforms. Computers and Geosciences, 26,779–793.
24. Upadhyay, D., Jahn-Awe, S., Pin, C., Paquette, J.L., and Braun, I. (2006) Neoproterozoic alkaline magmatism at Sivamalai, Southern India. Gondwana Research, 10, 156–166.
25. Zhang, J., Zhao, G., Sun, M., Wilde, S.A., Li, S., and Liu, S. (2006) High-pressure mafic granulites in the Trans-North China Orogen: Tectonic significance and age. Gondwana Research, 9, 349–362.